MICROBIOLOGY

A dual-mechanism luminescent antibiotic for bacterial infection identification and eradication

Guobin Qi[1]†, Xianglong Liu[1,2]†, Hao Li[3]†, Yunyun Qian[3], Can Liu[4], Jiahao Zhuang[1,2], Leilei Shi[5]*, Bin Liu[1,2,6]*

Because of the rapid emergence of antibiotic-resistant bacteria, there is a growing need to discover antibacterial agents. Here, we design and synthesize a compound of TPA2PyBu that kills both Gram-negative and Gram-positive bacteria with an undetectably low drug resistance. Comprehensive analyses reveal that the antimicrobial activity of TPA2PyBu proceeds via a unique dual mechanism by damaging bacterial membrane integrity and inducing DNA aggregation. TPA2PyBu could provide imaging specificity that differentiates bacterial infection from inflammation and cancer. High in vivo treatment efficacy of TPA2PyBu was achieved in methicillin-resistant *Staphylococcus aureus* infection mouse models. This promising antimicrobial agent suggests that combining multiple mechanisms of action into a single molecule can be an effective approach to address challenging bacterial infections.

INTRODUCTION

The rise of antibiotic resistance poses a severe global health threat that is anticipated to worsen in the foreseeable future (*1*–*3*). In addition, the declining discovery of antibiotics coupled with a nearly exhaustion of the antibiotics development pipeline is exacerbating this already dire issue (*4*, *5*). It is estimated that the annual death toll due to resistant infections will reach 10 million by 2050 if no immediate action is taken to discover and develop antibiotics (*6*). Recent initiatives have aimed to revitalize antibiotics research, yet most of the progress has involved modifying existing antibiotics or developing compounds that function via similar mechanisms of action to those of conventional antibiotics (*7*–*9*). In general, antibacterial agents targeting a single site are highly prone to developing resistance, as a single-step mutation in the drug target can lead to a considerable reduction in the drug efficacy. Conversely, antibacterial agents that target more than one molecular site or with a "physical" mechanism of action, such as disrupting bacterial cell membranes, have a low likelihood for the development of high-level endogenous resistance (*10*–*12*). Hence, there is a strong need for innovating classes of antibacterial agents with more than one mechanism of action and well tolerated with a low propensity for resistance development.

In addition to the challenges associated with antibiotic development, another major hurdle in the treatment of bacterial infections lies in the accurate identification and localization of the infections. This difficulty arises from the fact that the symptoms of bacterial infections often overlap with a variety of other diseases, such as inflammation and cancer (*13*). This often results in the inappropriate and empirical use of antibiotics, accelerating the development of drug resistance. Tracers for bacterial infections offer a solution to diagnostic challenges in specific clinical scenarios, such as distinguishing infection from sterile inflammation in implant-associated conditions, as inflammation markers often reflect the body's response to the implant rather than the presence of an infection. Therefore, strategies that can specifically differentiate bacterial infection from inflammation and cancer are highly desirable, which have been seldom reported (*14*, *15*). Past efforts to identify bacteria have focused largely on nuclear and fluorescent techniques based on radiotracers and fluorophores derived from peptides, antibiotics, and sugars (*14*, *16*–*19*). Still, no bacterial imaging agent is routinely used in clinics. Recently, a class of fluorogenic molecules that emit strong fluorescence in aggregate state or upon binding with analysts has attracted increasing attention in biomedical applications (*20*–*22*). These molecules with aggregation-induced emission (AIE) have been equipped with photosensitive properties to facilitate imaging-guided photodynamic bacteria eradication (*23*–*26*). Despite the effective photodynamic bactericidal capabilities, the challenge of limited light penetration restricts their widespread applications (*27*). Therefore, it will be ideal to develop luminogens that can identify bacterial infections and kill them like antibiotics, with a low frequency of drug resistance.

In this contribution, we report the design and synthesis of TPA2PyBu to kill both Gram-positive and Gram-negative bacteria, including drug-resistant bacterial pathogens such as multidrug-resistant *Escherichia coli* (MDR *E. coli*) and methicillin-resistant *Staphylococcus aureus* (MRSA USA300), through a distinctive dual-mechanism of action with low frequencies of detectable resistance. Detailed analyses using microscopy and bioassay techniques revealed that TPA2PyBu could kill bacteria via damaging bacterial membrane integrity and inducing DNA aggregation (Fig. 1). Moreover, TPA2PyBu exhibited strong emission upon inserting the bacterial DNA but showed low emission after interacting with the cell membrane. Therefore, in a bacterial infection animal model, TPA2PyBu could identify bacterial infection from other diseases including chemical inflammation and cancer. Meanwhile, TPA2PyBu has been demonstrated to be effective in treating MRSA infection in vivo. This study suggests that combining more than one mechanism of action into a single chemical scaffold may be an underappreciated approach to targeting challenging bacterial pathogens.

[1]Department of Chemical and Biomolecular Engineering, National University of Singapore, 4 Engineering Drive 4, Singapore 117585, Singapore. [2]Joint School of the National University of Singapore and Tianjin University, International Campus of Tianjin University, Binhai New City, Fuzhou 350207, China. [3]Department of Organ Transplantation, Xiang'an Hospital of Xiamen University, School of Medicine, Xiamen University, Xiamen, 361005, Fujian, China. [4]Department of Spine Surgery, Center for Orthopedic Surgery, The Third Affiliated Hospital of Southern Medical University, Guangzhou 510515, China. [5]Precision Research Center for Refractory Diseases in Shanghai General Hospital, Shanghai Jiao Tong University School of Medicine, Shanghai 200025, China. [6]Institute for Functional Intelligent Materials, National University of Singapore (Singapore), Blk S9, Level 9, 4 Science Drive 2, Singapore 117544, Singapore.
*Corresponding author. Email: leilei.shi@shgh.cn (L.S.); cheliub@nus.edu.sg (B.L.)
†These authors contributed equally to this work.

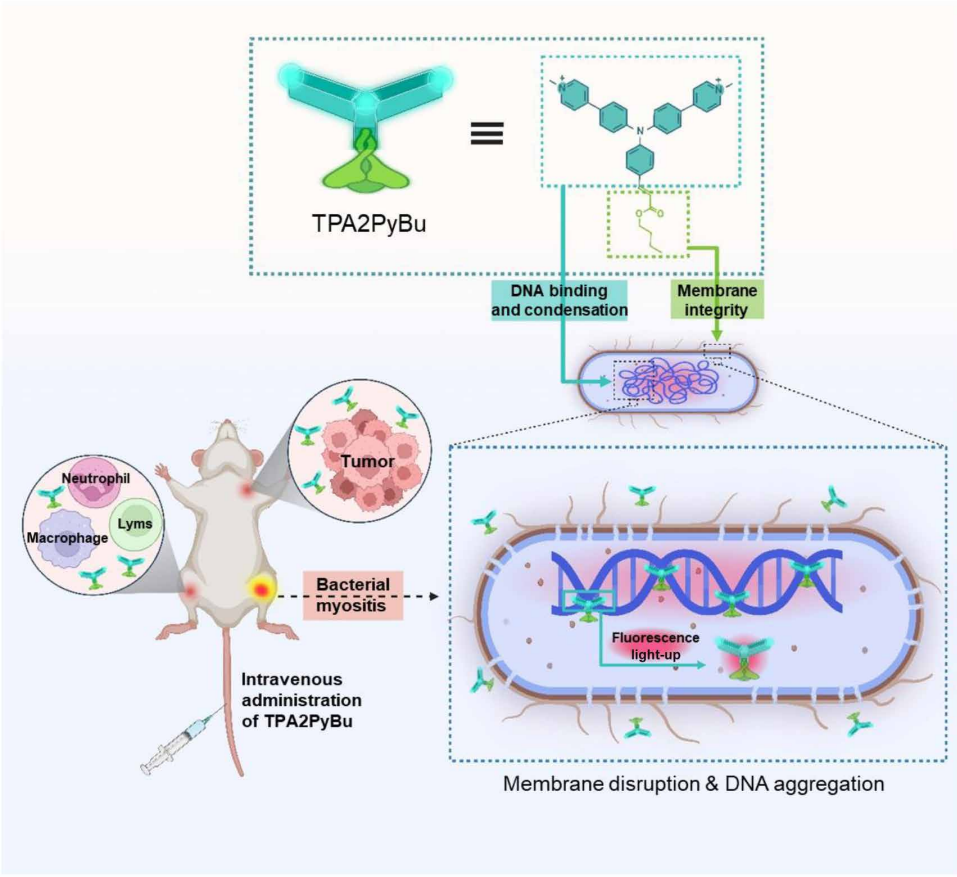

Fig. 1. TPA2PyBu and its function to image and kill bacteria. Structure of TPA2PyBu and schematic representation of the experimental approach for imaging mice injected with either *S. aureus*, tumor, and sterile myositis and subsequent detection of bacterial infection with TPA2PyBu. Lyms, lymphocytes.

RESULTS

Molecular design, synthesis, and photophysical properties

An ideal luminogen capable of discerning bacterial infections from other diseases, such as inflammation and tumors, requires specific fluorescence change upon interaction with bacteria while avoiding interactions with cells or tissues. The current antibacterial mechanisms of existing antibiotics include inhibition of cell wall synthesis, DNA replication and transcription, protein synthesis, etc. To screen a luminogen that recognizes and kills bacteria, a series of molecules TPA2PyCHO, TPA2PyMe, TPA2PyEt, TPA2PyBu, and TPA2PyHex was elaborately designed and synthesized (Fig. 2A). Briefly, these molecules were synthesized from 4-(bis(4-(pyridin-4-yl)phenyl)amino)benzaldehyde, which underwent bromination in the presence of *N*-bromosuccinimide to offer compound **1** as a yellow solid in 89.9% yield. Compound **1** was then treated with pyridin-4-ylboronic acid via Suzuki reaction to offer compound **2** as a yellow solid in 71.9% yield. The subsequent reaction between compound **2** and iodomethane through a methylation reaction afforded compound **3** (TPAPyCHO) as an orange solid in 95% yield. Last, compound **3** was reacted with compound **5** to offer TPA2PyMe, TPA2PyEt, TPA2PyBu, and TPA2PyHex with good yields from 80 to 85%. All the intermediates and final molecules were well characterized by ^{1}H nuclear magnetic resonance (NMR), ^{13}C NMR, and mass spectrometry (figs. S1 to S15).

The optical properties of TPA2PyCHO, TPA2PyMe, TPA2PyEt, TPA2PyBu, and TPA2PyHex are shown in Fig. 2B. These compounds exhibit a similar absorption profile in water with the absorption maximum located in the range of 350 to 500 nm. The compounds have an emission maximum at around 632 nm, which yielded a large Stokes shift of 200 nm (Fig. 2C). Next, we used a mixed solvent [dimethyl sulfoxide (DMSO)/toluene] with different toluene fractions to evaluate the optical properties of TPA2PyCHO, TPA2PyMe, TPA2PyEt, TPA2PyBu, and TPA2PyHex. As shown in Fig. 2 (D and E), the DMSO solutions of these compounds exhibited very weak emissions, and the fluorescence was gradually intensified with the increased proportion of toluene in the solvent mixture. During this process, a slight blueshift of the emission maximum was observed for these compounds in 99% [toluene in DMSO (v/v)] solution as compared to that in 100% DMSO, which should be attributed to the twisted intramolecular charge transfer effect. Meanwhile, these compounds have shown weak fluorescence in water due to their good dispersity in aqueous media. These results indicate that the compounds have AIE properties.

Having demonstrated that these molecules displayed AIE properties, we moved on to investigate their interactions with DNA through fluorescence titration experiments. As shown in Fig. 2F, for TPA2PyCHO, TPA2PyMe, TPA2PyEt, TPA2PyBu, and TPA2PyHex, addition of circulating tumor DNA (ctDNA) to each solution led to a fluorescence enhancement of 14-, 32-, 94-, 102-, and 70-fold as compared to their intrinsic fluorescence in aqueous media.

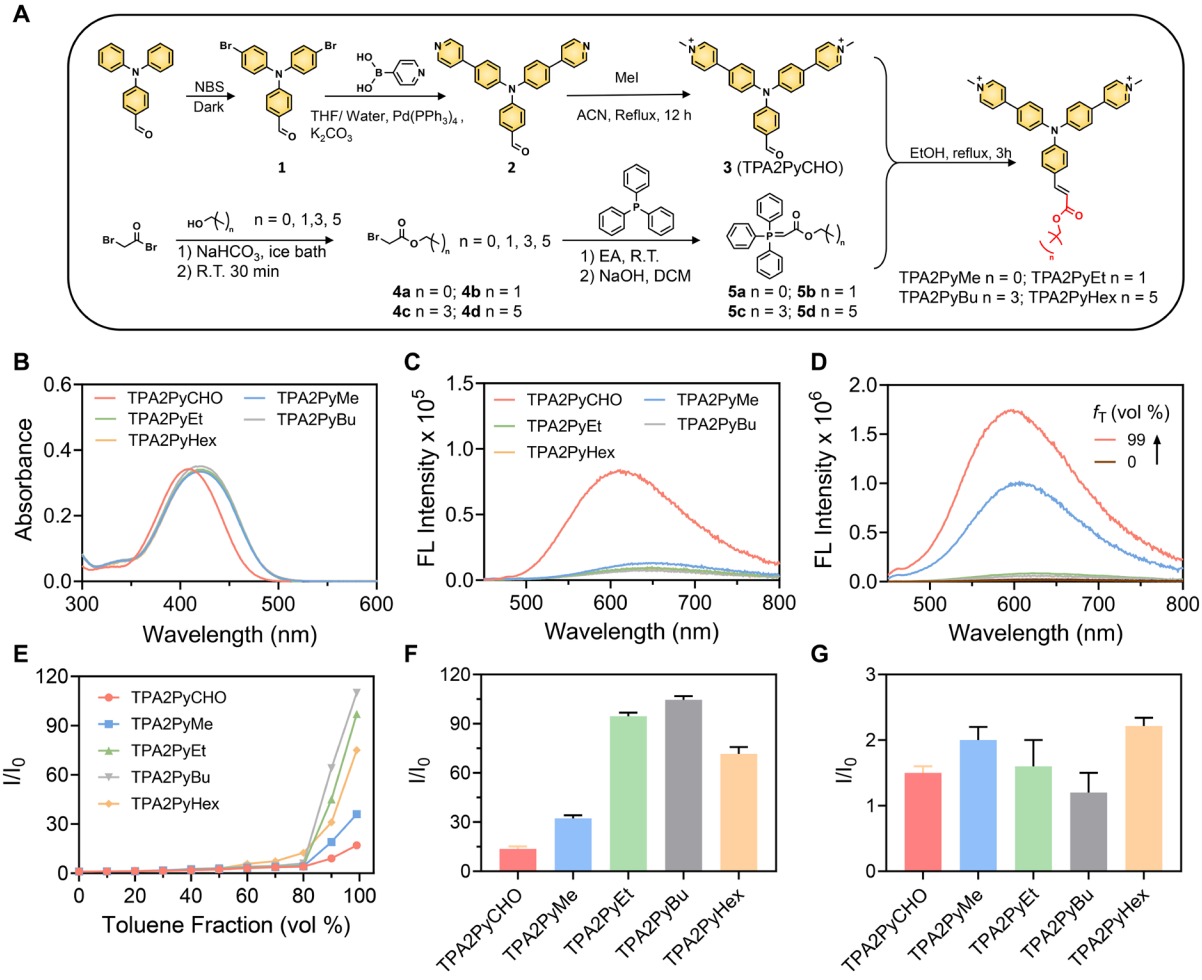

Fig. 2. Synthetic route and photophysical properties of TPA2PyCHO, TPA2PyMe, TPA2PyEt, TPA2PyBu, and TPA2PyHex. (**A**) Synthetic route of TPA2PyCHO, TPA2PyMe, TPA2PyEt, TPA2PyBu, and TPA2PyHex. (**B**) UV-vis absorption spectra of TPA2PyCHO, TPA2PyMe, TPA2PyEt, TPA2PyBu, and TPA2PyHex in an aqueous solution with a concentration of 10 μM. (**C**) Fluorescence (FL) spectra of TPA2PyCHO, TPA2PyMe, TPA2PyEt, TPA2PyBu, and TPA2PyHex in an aqueous solution with a concentration of 10 μM. (**D**) FL spectra of TPA2PyBu (10 μM) in DMSO/toluene mixtures. (**E**) Plots of the relative emission intensity of TPA2PyCHO, TPA2PyMe, TPA2PyEt, TPA2PyBu, and TPA2PyHex versus toluene fraction. I_0 and I are the peak values of fluorescence intensities of compounds (10 μM) in DMSO and DMSO/toluene mixtures, respectively. (**F**) The relative emission intensity of TPA2PyCHO, TPA2PyMe, TPA2PyEt, TPA2PyBu, and TPA2PyHex (10 μM) after the addition of ctDNA (2 μg/ml). I_0 and I are the peak values of fluorescence intensities of compounds in water and DNA mixtures, respectively. (**G**) The relative emission intensity of TPA2PyCHO, TPA2PyMe, TPA2PyEt, TPA2PyBu, and TPA2PyHex (10 μM) after the addition of DOPC (2 μg/ml). I_0 and I are the peak values of fluorescence intensities of compounds (10 μM) in water and DOPC mixtures, respectively. THF, tetrahydrofuran; h, hours, R.T., room temperature; EtOH, ethanol.

However, only a weak fluorescence enhancement (<3-fold) was observed when dioleoylphosphatidylcholine (DOPC) was added into the same aqueous solutions (Fig. 2G). The increase in fluorescence intensity results from the strong interaction between these compounds and ctDNA, which is primarily driven by electrostatic forces and groove binding. These interactions restrict the intramolecular motions of the molecules and consequently activating their fluorescence process (fig. S16). As TPA2PyBu shows the best selectivity between ctDNA and DOPC, we also investigated the fluorescence changes of TPA2PyBu incubated with other potential interferents in biological systems, including bovine serum albumin, red blood cells, raw 264.7, and NIH/3T3 (figs. S17 to S19). The fluorescence intensity was only slightly enhanced upon mixing with different biomacromolecules, indicating its good potential for in vivo applications.

Antimicrobial activity

To assess the potential of TPA2PyCHO, TPA2PyMe, TPA2PyEt, TPA2PyBu, and TPA2PyHex as effective antimicrobial agents, we determined the minimal inhibitory concentration (MIC) of these compounds toward both Gram-positive and Gram-negative bacteria, including clinically relevant pathogens. In this study, MIC was defined as the lowest concentration of the compound that results in no visible bacterial growth after 14 hours of incubation at 37°C. As shown in Fig. 3A and fig. S20, TPA2PyCHO, TPA2PyMe, and TPA2PyEt exhibited a general bacterial growth inhibition activity against *S. aureus* and MRSA with MICs in the range of 5 to 10 μM, while these three compounds showed poor bacterial growth inhibition toward *E. coli*. In contrast, both TPA2PyBu and TPA2PyHex demonstrated marked inhibition of growth across multiple strains of Gram-positive and Gram-negative pathogens including

A

		MIC (μM)				
		TPA2PyCHO	TPA2PyMe	TPA2PyEt	TPA2PyBu	TPA2PyHex
Gram positive	*S. aureus*	10	5	5	1	1
	MRSA	10	10	5	1	1
Gram negative	*E. coli*	>50	50	50	5	5
	MDR *E. coli*	>50	>50	>50	10	10

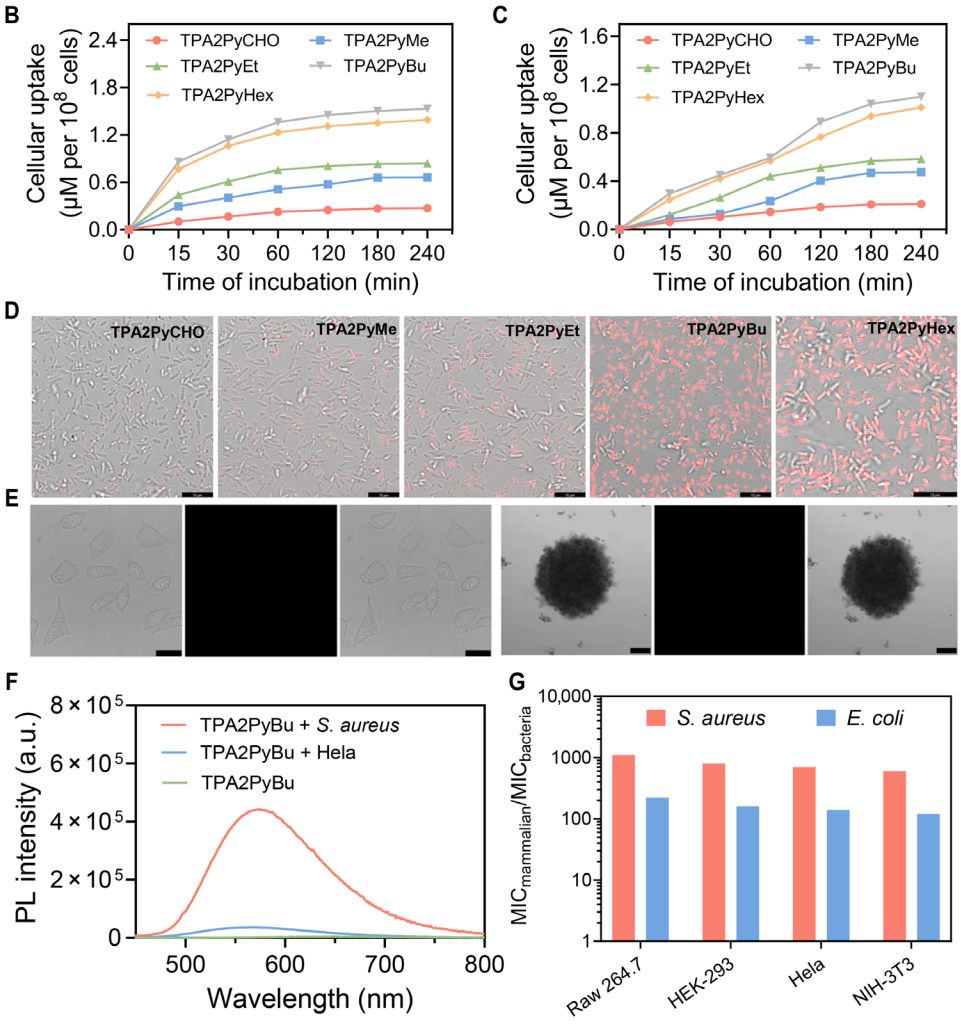

Fig. 3. Antibacterial and bacterial binding properties of TPA2PyCHO, TPA2PyMe, TPA2PyEt, TPA2PyBu, and TPA2PyHex. (**A**) Antibacterial activities (MIC) of TPA2PyCHO, TPA2PyMe, TPA2PyEt, TPA2PyBu, and TPA2PyHex against *S. aureus*, *E. coli*, MRSA, and MDR *E. coli*. Time course of uptake in the *S. aureus* (**B**) and *E. coli* (**C**) in terms of concentration of TPA2PyCHO, TPA2PyMe, TPA2PyEt, TPA2PyBu, and TPA2PyHex per colony-forming units (CFU × 10^8). (**D**) Confocal images of *E. coli* upon incubation with TPA2PyCHO, TPA2PyMe, TPA2PyEt, TPA2PyBu, and TPA2PyHex at a concentration of 2 μM. Scale bars, 10 μm. (**E**) Confocal images of Hela (scale bars, 25 μm) and 3D Hela spheroid (scale bars, 100 μm) upon incubation with TPA2PyBu (2 μM). (**F**) PL spectra of TPA2PyBu (2 μM) upon incubation with *S. aureus* and mammalian cells in PBS. (**G**) The therapeutic index of TPA2PyBu was determined by (MIC against the indicated mammalian cell line)/(MIC against *S. aureus* or *E. coli*). a.u., arbitrary units.

MRSA and MDR *E. coli* with MICs in the range of 1 to 10 μM. Meanwhile, both TPA2PyBu and TPA2PyHex displayed comparable inhibitory efficacy against *S. aureus* MRSA USA300, a clinical isolate. Moreover, the MICs of TPA2PyBu toward *Pseudomonas aeruginosa*, *Acinetobacter baumannii*, and *Enterococcus faecium* were also evaluated. Figure S21 shows that TPA2PyBu exhibits broad-spectrum antibacterial activity, with MIC values of 50, 2, and 5 μM against *P. aeruginosa*, *A. baumannii*, and *E. faecium*, respectively, indicating high antimicrobial activity toward *A. baumannii* and *E. faecium* but lower antimicrobial activity toward *P. aeruginosa*. This observation suggests that the inhibitory activity of these compounds is not limited to a specific bacterial species.

To further understand the influence of the alkyl chain length, we conducted a cell uptake experiment to investigate the internalization of TPA2PyCHO, TPA2PyMeth, TPA2PyEthyl, TPA2PyBu, and TPA2PyHex in Gram-positive *S. aureus* and Gram-negative *E. coli* in phosphate-buffered saline (PBS) media. *S. aureus* and *E. coli* were incubated with 2 μM of each compound for different times. The supernatant was collected and analyzed by an ultraviolet-visible (UV-vis) spectrophotometer. As shown in Fig. 3 (B and C), after incubation with bacteria, the absorption of TPA2PyBu and TPA2PyHex in the supernatant decreased markedly, indicating that most of TPA2PyBu and TPA2PyHex were taken up by both *S. aureus* and *E. coli* cells. On the contrary, an overall lower level of uptake of TPA2PyCHO, TPA2PyMeth, and TPA2PyEth by bacteria was observed as compared with that of TPA2PyBu and TPA2PyHex. This is largely attributed to the increase in alkyl chain length that can be advantageous in terms of membrane interaction, facilitating membrane penetration. This also explains why TPA2PyBu and TPA2PyHex exhibit high inhibitory activity compared with that of TPA2PyCHO, TPA2PyMe, and TPA2PyEt. In addition, for Gram-positive *S. aureus*, the uptake of these compounds reached saturation within 60 min, but Gram-negative *E. coli* required a longer time to reach saturation, due to the existence of poor penetration outer membrane that limits the penetration of these compounds. Meanwhile, confocal laser scanning microscopy (CLSM) was used to monitor the cell uptake by incubating them with *E. coli* cells. As shown in Fig. 3D, *E. coli* exhibited weak fluorescent signals upon incubation with TPA2PyCHO, TPA2PyMe, and TPA2PyEt at a concentration of 2 μM, indicating a low penetration of these compounds into *E. coli* cells. However, strong fluorescence was observed in *E. coli* after incubation with TPA2PyBu and TPA2PyHex, implying good penetration of TPA2PyBu and TPA2PyHex into *E. coli* cells. Meanwhile, both *S. aureus* and *E. coli* exhibited more internalization of TPA2PyBu compared to that of TPA2PyHex (Fig. 3, B and C). Therefore, TPA2PyBu was selected to conduct the subsequent experiments.

Next, we conducted time- and concentration-dependent killing assays to elucidate whether its mode of action involves bactericidal or bacteriostatic mechanisms. Under nutrient-rich growth conditions with an initial bacterial cell density of 1×10^6 colony-forming units (CFU)/ml (fig. S22), we observed substantial bacterial cell death in the presence of TPA2PyBu, suggesting that its mode of action is bactericidal. Subsequently, we investigated the potential of TPA2PyBu to induce bacterial cell death under metabolically repressed and antibiotic-tolerant conditions (figs. S23 and 24). By culturing *S. aureus* in a nutrient-free buffer supplemented with TPA2PyBu, we observed that this molecule retained its bactericidal activity, indicating its effectiveness against nongrowing bacteria and antibiotic tolerant. Since TPA2PyBu can interact with bacterial cells and show strong fluorescent signals, we next used the fluorescent colocalization approach for the identification of the TPA2PyBu target. Specifically, *S. aureus* and MRSA treated with TPA2PyBu and subsequently costained with Hoechst were monitored by CLSM. As shown in fig. S25, obvious red fluorescent signals from TPA2PyBu were detected in both *S. aureus* and MRSA cells, which were well overlaid with the blue emissions from Hoechst. These results indicated that TPA2PyBu could enter bacterial cells to yield fluorescence light-up.

An effective antibacterial agent should have the ability to specifically target pathogenic bacteria while sparing mammalian hosts from harm. To investigate the specificity of TPA2PyBu to bacteria, the fluorescence changes of TPA2PyBu upon incubation with *S. aureus* and mammalian cells, HeLa cells were monitored. As shown in Fig. 3F, the fluorescence intensity of TPA2PyBu was slightly enhanced upon incubation with HeLa cells, which was much weaker compared to that upon incubation with *S. aureus*, indicating weak interactions between TPA2PyBu and HeLa cells. To visually investigate the interactions between TPA2PyBu and mammalian cells, CLSM was used to monitor the fluorescence distribution of TPA2PyBu in HeLa cells and three-dimensional (3D) HeLa spheroid. As shown in Fig. 3E, almost no fluorescence was observed on HeLa cells and 3D HeLa spheroid at the low concentration (2 μM), which was effective for labelling *S. aureus*. Following that, we examined the concentrations of TPA2PyBu necessary to inhibit the growth of different mammalian cell lines. Notably, TPA2PyBu showed promising results with Raw 246.7 cells, human embryonic kidney (HEK) 293, HeLa, and NIH/3T3, as evidenced by their requirement of doses more than 100 times higher for growth inhibition compared to those needed for killing *E. coli* and *S. aureus* (Fig. 3G).

Antimicrobial mechanism

Having demonstrated that TPA2PyBu could act as an effective antimicrobial reagent, we moved on to investigate its mechanism of action. To determine how TPA2PyBu affects the bacterial nucleoid morphology in live cells, bacterial cytological profiling, a rapid approach for identifying the cellular pathway affected by antibacterial molecules, was used to provide information on the mechanism of action of TPA2PyBu. *S. aureus* and *E. coli* were subjected to a 2-hour treatment with 2 × MIC of TPA2PyBu, followed by staining with Hoechst and FM6-64 to show nucleoid morphology and membrane morphology, respectively. The cells were subsequently imaged using CLSM. As shown in Fig. 4A, it is observed that the nucleoid is uniformly distributed in both *S. aureus* and *E. coli* cells without any treatment. In contrast, the nucleoid in *S. aureus* and *E. coli* showed a state of aggregation after treatment with TPA2PyBu. These results indicated that TPA2PyBu-induced DNA aggregation is directly related to its antibacterial effect.

Having demonstrated that TPA2PyBu could penetrate bacterial cell membrane and bind with DNA, we further evaluated whether TPA2PyBu could affect bacterial membrane integrity. The membrane potential and permeability of *E. coli* were measured using flow cytometry to monitor the fluorescence shift in the presence of $DiOC_2(3)$ and TO-PRO-3 upon treatment with TPA2PyBu (*28*). As a cationic dye, $DiOC_2(3)$ forms bright and red fluorescent aggregates with increasing membrane potential while emitting green fluorescence upon the decreased membrane potential. The spectral shifts in these cells provided a measure of membrane potential. On the other hand, TO-PRO-3 is an excellent far red fluorescent nucleic acid stain that is impermeant to live cells but accumulates in cells with compromised membranes, making it a useful indicator for the measurement of membrane permeability. As a positive control, a membrane-decoupler (CCCP) and a pore-forming antibacterial peptide (nisin) were chosen to monitor the fluorescence change of treated bacterial cells. As shown in Fig. 4B, we observed the expected shift in $DiOC_2(3)$ staining using CCCP, while no changes were observed in TO-PRO-3 staining using CCCP, as CCCP only affected membrane potential but not permeability. Meanwhile, we observed the expected shifts in both $DiOC_2(3)$ and TO-PRO-3 upon treatment with nisin, as nisin could disrupt both membrane potential and permeability. As a negative control, ciprofloxacin, an antibiotic with no specific interaction with the membrane, exhibited no

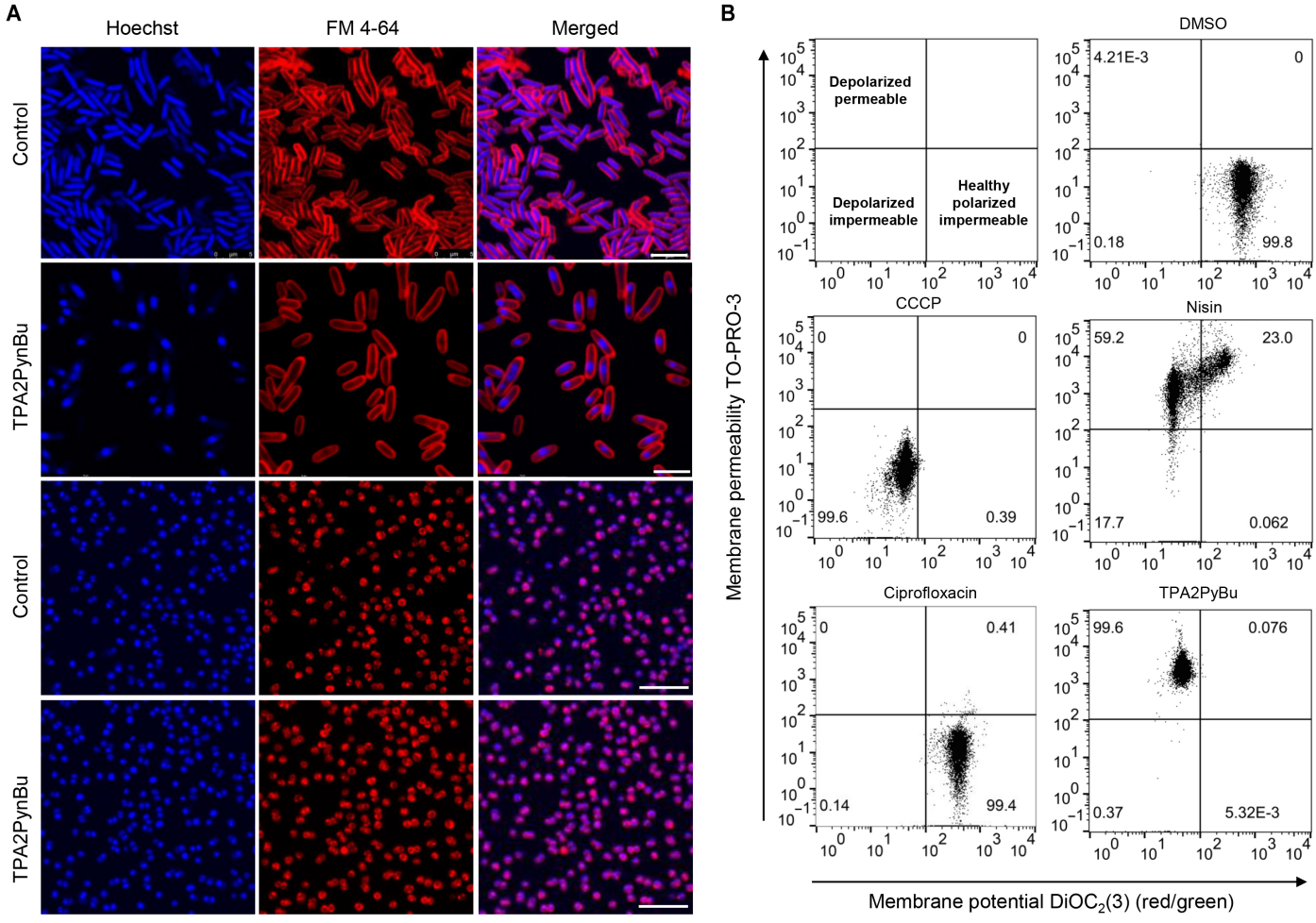

Fig. 4. Effect of TPA2PyBu treatment on bacterial cell morphology and membrane integrity. (**A**) Confocal images of *S. aureus* and *E. coli* cells treated with TPA2PyBu. Cells were treated for 30 min with 2 × MIC of TPA2PyBu. Hoechst, blue; FM4-64, red. Scale bars, 5 μm. (**B**) Flow cytometry results of *E. coli* cells upon treatment with PBS (containing 1% DMSO), CCCP (5 μM), nisin (25 μg/ml, 2 × MIC), ciprofloxacin (1 μM, 2 × MIC), and 10 μM TPA2PyBu (2 × MIC) for 30 min, followed by staining with $DiOC_2(3)$ and TO-PRO-3.

observable alteration in the staining of $DiOC_2(3)$ and TO-PRO-3. After treatment with TPA2PyBu for 30 min, subsequent staining with $DiOC_2(3)$ and TO-PRO-3 showed obvious defects in both membrane polarization and permeability. These results suggest that TPA2PyBu disrupts both membrane potential and permeability barrier.

To understand the antibacterial mechanism of TPA2PyBu, the gene expression variations between TPA2PyBu-treated and untreated groups were investigated via a comparative transcriptome study on *S. aureus*. In this study, the differentially expressed genes (DEGs) were screened out with a cutoff value $\log_2$(fold change) > 1 or $\log_2$(fold change) < −1 and a *P* value < 0.05. As shown in Fig. 5A, compared to the untreated groups, 46 DEGs were identified with 43 up-regulated and 3 down-regulated genes in TPA2PyBu-treated groups. Among the 46 DEGs, ~24% DEGs were associated with metabolism processes, including galactose metabolism, atrazine degradation, nickel cation binding, and other metabolism processes. In addition, about 17% of DEGs were associated with cell membrane structure and function, such as transmembrane transport, transferase activity, and adenosine triphosphatase activity. Meanwhile, there are 8% DEGs related to DNA binding and damage repair. Among the down-regulated genes, *SAOUHSC_01788* stands out as it has been reported to be involved in key metabolic pathways such as glycine, serine, and threonine metabolism, as well as aminoacyl-tRNA biosynthesis (*29*). As a gene that is potentially vital for the survival of *S. aureus* (*29*), the substantial down-regulation of *SAOUHSC_01788* underscores the impact of TPA2PyBu on bacterial metabolism at the genetic level. In addition, in the Kyoto Encyclopedia of Genes and Genomes (KEGG) enrichment results (Fig. 5B), prominent enrichment was observed in bacterial metabolic pathways, including galactose metabolism, arginine biosynthesis, kinases, and protein transport pathways. To further understand the biological significances of the DEGs, gene ontology (GO) enrichment analysis was carried out. As shown in Fig. 5C, the GO enrichment results revealed that DEGs were enriched in the phosphotransferase system (PTS) which mediated sugar transport and phosphorylation in bacteria (*30*–*32*). Meanwhile, prominent DEG enrichment in nickel cation binding, indicating bacterial metabolism, was altered to adapt to the treatment of TPA2PyBu (*33*). These results indicated that TPA2PyBu enhanced bactericidal activity by influencing the regulatory network and metabolic pathways associated with PTS.

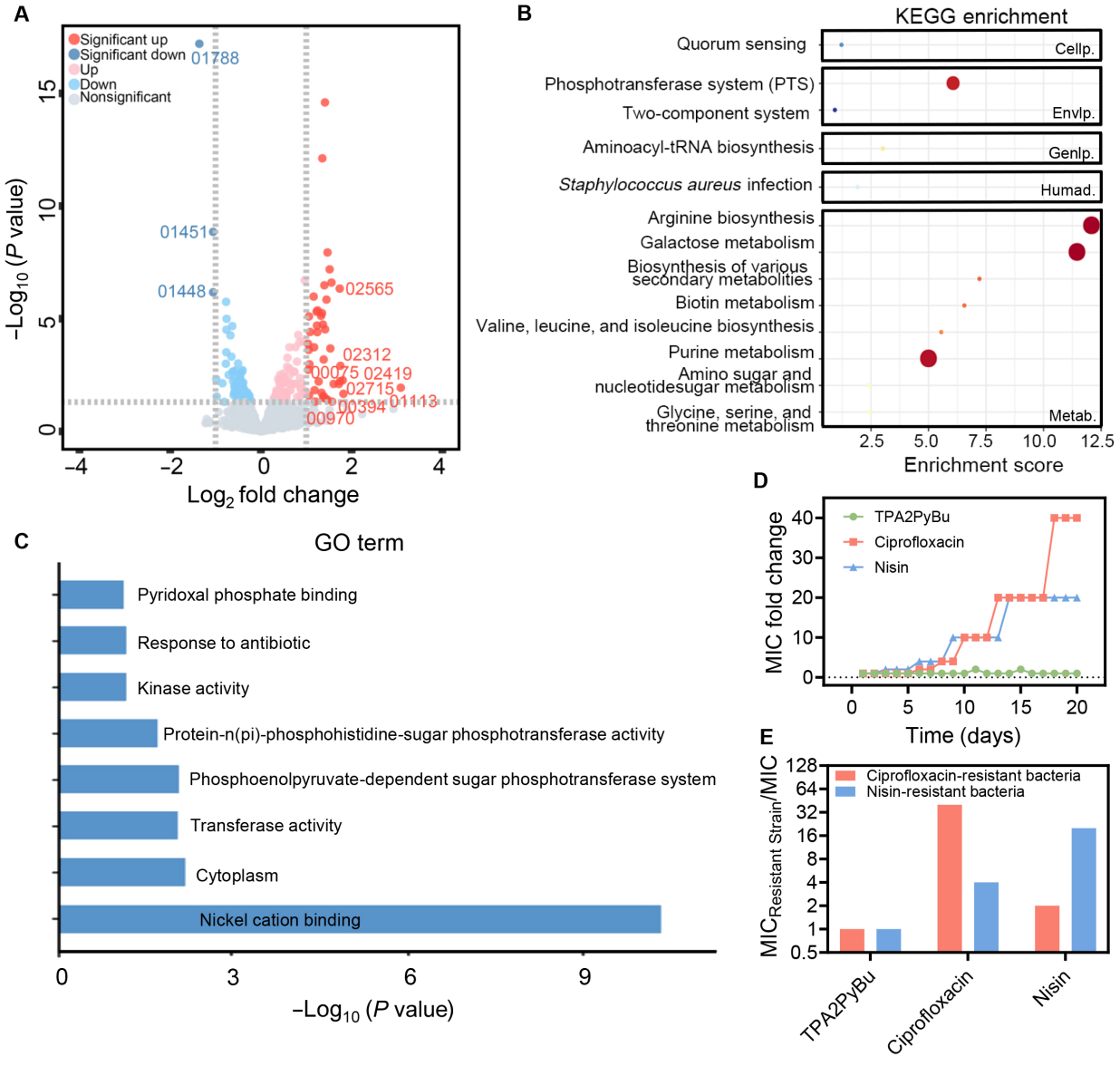

Fig. 5. RNA sequencing and drug resistance. (**A** and **B**) Screening of DEGs in *S. aureus* induced by TPA2PyBu treatment: (A) volcano plots of the DEGs between TPA2PyBu-treated groups and untreated groups. KEGG pathways (B) and GO enrichment (**C**) of the up- and down-regulated DEGs. (**D**) Drug resistance development profiles of *S. aureus* MRSA USA300 after exposure to TPA2PyBu, ciprofloxacin, and nisin at sub-MIC after 20 days of passage in liquid LB media. (**E**) MIC fold changes of *S. aureus* MRSA USA300 mutants to TPA2PyBu, ciprofloxacin, and nisin. The mutants resistant to ciprofloxacin and nisin were isolated from serial passaging in respective antibiotics.

To further assess the potential of TPA2PyBu as an antibiotic, we attempted to investigate the likelihood of bacteria developing resistance to this compound. For this purpose, *S. aureus* MRSA USA300 was used for drug resistance studies. Upon plating 1×10^8 CFU of *S. aureus* MRSA USA300 onto agar containing 4 μM TPA2PyBu (4 × MIC), we were unable to isolate stable TPA2PyBu-resistant mutants. To quantitatively investigate the resistance rates, *S. aureus* MRSA USA300 cells were treated with TPA2PyBu for 20 serial passages at sub-MIC, and MIC was determined in each passage of the bacteria. Meanwhile, two antibiotics, nisin and ciprofloxacin, were used as the control. As shown in Fig. 5D, repeated use of TPA2PyBu did not cause resistance development in *S. aureus* MRSA USA300 even after 20 passages, while multiple treatments with nisin or ciprofloxacin successfully isolated mutants resistant to both the control antibiotics. Throughout the experiment, the resistance to nisin and ciprofloxacin exhibited a gradual increase, whereas the resistance level to TPA2PyBu remained constant. This suggested that these bacteria did not develop partial resistance to TPA2PyBu. Furthermore, we also demonstrated that the mutants evolving resistance to antibiotics such as nisin and ciprofloxacin did not exhibit cross-resistance to TPA2PyBu (Fig. 5E). The low frequency of resistance to TPA2PyBu could be the result of its dual mechanisms of action.

In vivo bacterial imaging and antibacterial activity

Given that TPA2PyBu exhibits fluorescence light up activity upon interaction with bacteria, we subsequently investigated whether TPA2PyBu had the ability to image bacterial infections in the mouse.

S. aureus and saline were inoculated in the right and left thigh muscles of the mice, respectively. Twelve hours after inoculated with *S. aureus*, the mice were intravenously injected with TPA2PyBu [TPA2PyBu (40 μg kg^{-1})in PBS]. After an additional 6 hours, the fluorescence imaging was carried out in an IVIS imaging system. As shown in Fig. 6A, a strong fluorescent signal was observed at *S. aureus*–infected site, while there was no fluorescence at the saline injection site. Specifically, *S. aureus*–infected tissue displayed a 31-fold increase in fluorescence intensity as compared with that from the uninfected controls (Fig. 6B), enabling convenient in vivo visualization of the infected area. We further quantified the in vivo targeting capability of TPA2PyBu toward bacteria by performing a biodistribution study of TPA2PyBu in mice infected with *S. aureus*. As shown in Fig. 6C, the average fluorescent signals in infected tissues are increased by 17- to 69-fold as compared to those in uninfected tissues and major organs. This suggests that it has the potential to be used for imaging bacterial infections in a variety of tissues.

Inspired by the encouraging in vivo experimental results, we proceeded to explore the imaging specificity of TPA2PyBu in distinguishing three potentially overlapping diagnoses: infection, inflammation, and cancer. Developing molecular probes with high specificity for bacteria has been challenging, as many probes also tend to accumulate in inflamed and cancerous tissues (*34*–*36*). To assess the specificity of TPA2PyBu for bacterial infection, we devised an experiment wherein bacterial infection, inflammation, and tumor were implanted in distinct regions of the same mouse. The HeLa cervical cancer cells were inoculated in the right shoulder region, turpentine was injected in the left hindlimb, and live *S. aureus* was injected (1×10^8 CFU) in the right hindlimb as illustrated in Fig. 6D. After 12 hours, the mice were intravenously injected with TPA2PyBu [TPA2PyBu (40 μg kg^{-1}) in PBS] and imaged at the set time points (1, 2, 4, and 6 hours postinjection). As shown in Fig. 6 (D and E), no obvious fluorescent signals were observed in sterile/chemical inflammation with turpentine and the tumor sites at different times. However, the fluorescent signals in the *S. aureus*–infected muscles were continuously increased over time. These results reflected a preferential interaction of TPA2PyBu with the *S. aureus*–infected tissue. Meanwhile, because of the weak interaction of TPA2PyBu with tumors, macrophages, and biomolecules, the quantitative fluorescence intensity of *S. aureus*–infected tissue was notably higher than that of inflammation and tumor tissues. Up to a 26-fold increase in TPA2PyBu was observed for the bacteria infection–to–muscle ratio, whereas negligible signals were observed in inflammation or tumor (Fig. 6E), indicating that TPA2PyBu can distinguish bacterial infection from inflammation and cancers with high specificity.

Next, the in vivo bacteria clearance efficacy of TPA2PyBu was investigated in a subcutaneous infection mouse model included by *S. aureus* (1×10^8 CFU). After the infection had developed, TPA2PyBu (40 μg kg^{-1}), ciprofloxacin (40 μg kg^{-1}), and saline were administered via intravenous injection. Seven days postinjection, the infected tissues were collected and homogenized for the quantitative analysis of bacteria burden. The quantity of bacteria remaining in infected tissues was determined by CFU analysis (Fig. 6F). Compared to the saline-treated group, TPA2PyBu and ciprofloxacin showed a considerable reduction in bacteria CFUs, indicating that TPA2PyBu can be used to treat bacterial infection like antibiotics. Meanwhile, histological analysis was also carried out on the collected infection tissues. As illustrated in Fig. 6G, the hematoxylin and eosin (H&E) staining images showed that the infected tissue treated with TPA2PyBu exhibited minimal infiltration of inflammatory cells and normal skin structure in comparison to that of the control group. Last, we systematically investigated the in vivo toxicity of TPA2PyBu after intravenous injection. The levels of the important liver and kidney function biomarkers, such as aspartate aminotransferase, alanine aminotransferase, urea nitrogen, and creatinine, are like those in the control group, indicating no obvious hepatotoxicity and nephrotoxicity. For hematological analysis, white blood cells and lymphocytes in TPA2PyBu-treated groups were normal in comparison with the control groups (fig. S26). Subsequently, we also carried out histopathological analysis for major organs, including heart, lung, spleen, liver, and kidney. The H&E staining images showed no obvious organ damage (Fig. 6H). Overall, TPA2PyBu did not induce noticeable toxicity in vivo at the treatment dose, which showed great promise for it to be used as an antibiotic.

DISCUSSION

In conclusion, we have designed and synthesized a promising compound of TPA2PyBu, which is effective in killing both Gram-positive and Gram-negative bacteria. TPA2PyBu has a dual bactericidal mechanism with a low propensity for resistance development, a critical advantage in the fight against drug-resistant bacterial infections. Through bacterial cytological profiling, we confirmed that TPA2PyBu directly induces nucleoid aggregation, disrupting essential DNA functions. Quantitative flow cytometry using $DiOC_2(3)$ and TO-PRO-3 further revealed that TPA2PyBu compromises bacterial membrane integrity. The combination of these two distinct mechanisms likely contributes to the undetectably low frequency of resistance observed, as bacteria face simultaneous disruptions of nucleic acid processes and membrane function—two vital systems that are difficult to evade through single-step mutations. Beyond its bactericidal properties, TPA2PyBu demonstrated remarkable imaging specificity. Its strong interaction with bacterial cells allowed precise differentiation of bacterial infections from inflammation and cancer, addressing the critical need for contrast agents capable of accurate bacterial infection identification. This dual diagnostic and therapeutic capability positions TPA2PyBu as a valuable tool in infection management. The in vivo efficacy of TPA2PyBu in bacterial infection models underscores its potential for clinical application. Unlike many antimicrobial candidates that falter during the transition from in vitro to in vivo studies, TPA2PyBu has shown robust activity in complex biological systems. Nevertheless, further studies are required to confirm its safety profile, optimize dosing strategies, and assess long-tem outcomes before clinical applications.

The antibacterial activity of TPA2PyBu demonstrates promising efficacy against both Gram-positive and Gram-negative bacteria. Compared to previously reported AIE compounds, which primarily rely on photodynamic antibacterial mechanisms (*37*–*40*), most struggle to penetrate Gram-negative bacteria and require functional group modifications to target these pathogens effectively (*41*, *42*). While these AIE-based agents exhibit remarkable antibacterial activity under light irradiation, their photodynamic efficacy is heavily dependent on light exposure. This reliance on light, coupled with the limited penetration of light into tissues, poses challenges for their clinical translation. However, TPA2PyBu offers a unique combination of strong bactericidal activity, resistance suppression, and diagnostic specificity. These properties make it competitive in the field of antimicrobial AIE compounds, particularly as an innovative solution to the challenges posed by drug-resistant bacteria.

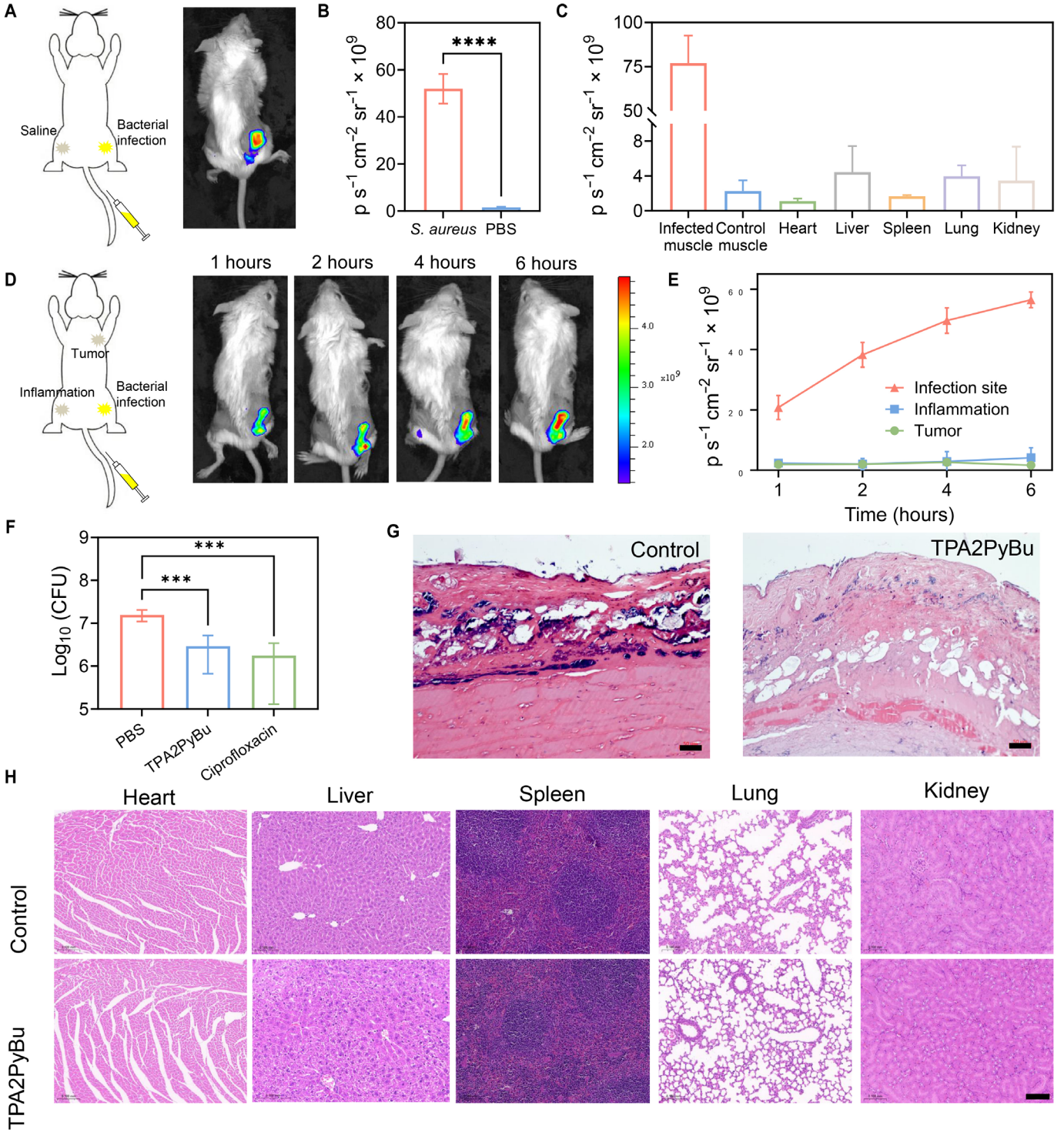

Fig. 6. In vivo imaging and killing of bacteria. (**A**) IVIS fluorescence images of a BALB/c mouse with *S. aureus*–induced myositis in the right hind limb at 6 hours after intravenous administration of TPA2PyBu (40 μg kg^{-1}) using PBS in the left limb as control. (**B**) Quantification of fluorescent signals in the site of bacterial myositis and control site. Bars represent the mean of three mice, and error bars display the SD. (**C**) Quantification of ex vivo fluorescence signals in tissues of bacterial myositis, noninfected tissue, and all the major organs. (**D**) Schematic of locations of infection, inflammation, and tumor in a BALB/c mouse. Fluorescence images of mice at different time points (1, 2, 4, and 6 hours) after intravenous administration of TPA2PyBu. (**E**) Quantification of average fluorescence intensities at the inflammation, tumor, and infected skin site treated with TPA2PyBu over time. (**F**) Number of bacterial colonies in the *S. aureus*–infected skin after treatment with PBS, TPA2PyBu, and ciprofloxacin. (**G**) Representative images of the infected skin slices after H&E staining upon treatment with PBS and TPA2PyBu. Scale bars, 50 μm. (**H**) H&E staining images of the major organs with or without TPA2PyBu injection. Scale bar, 100 μm. Mean ± SD, n = 3, ***$P < 0.001$, Statistical significance was analyzed via two-way ANOVA.

TPA2PyBu also has several favorable characteristics for drug development. Its strong fluorescence enables real-time imaging of bacterial interactions, a property valuable for diagnostic and therapeutic applications. Furthermore, its activity in MIC concentrations may reduce the likelihood of toxicity to human cells, an often-cited challenge in antimicrobial development. Moreover, the dual mechanism of action provides a clear advantage, as it reduces the likelihood of resistance development compared to traditional antibiotics. However, the stability of the TPA2PyBu in the presence of metabolic enzymes needs further evaluation to ensure that effective drug levels are maintained in vivo. Additional pharmacokinetic and pharmacodynamic studies are still required to evaluate its bioavailability and clearance rates in vivo.

Although TPA2PyBu exhibits potent activity against Gram-positive bacteria, including multidrug-resistant strains such as MRSA, activity against Gram-negative bacteria, although present, is less robust, especially for *P. aeruginosa*. The outer membrane of Gram-negative bacteria poses a major barrier, and our ongoing studies focus on modifications that enhance permeability through this membrane (*43*, *44*). Given the urgent need for Gram-negative-targeted antibiotics, improving this compound's efficacy against such pathogens is a priority. For instance, coupling with rigid groups to enhance the outer membrane penetration or structural adjustments to enhance lipopolysaccharide interaction may improve activity against Gram-negative bacteria (*45*, *46*).

The urgent need for innovative antimicrobial agents, particularly those effective against drug-resistant pathogens, underscores the significance of this work. TPA2PyBu represents a promising advancement in antimicrobial research, addressing key challenges in bacterial infection treatment and diagnosis. Its dual mechanism of action, diagnostic capabilities, and in vivo efficacy make it a compelling candidate for further preclinical and translational evaluation. Beyond its immediate antibacterial applications, TPA2PyBu may also serve as a platform for the development of multifunctional antimicrobial and diagnostic agents. With further optimization and evaluation, it has the potential to become a valuable addition to the arsenal against multidrug-resistant infections.

MATERIALS AND METHODS

Absorption and fluorescence spectra

The DMSO stock solutions of TPA2PyCHO, TPA2PyMe, TPA2PyEt, TPA2PyBu, and TPA2PyHex at a concentration of 1 mM were diluted in water to a concentration of 10 μM. Absorption spectra in the range of 300 to 800 nm were collected using H_2O in a cuvette as the blank for absorption measurement. The fluorescence spectra were collected in the range of 45 to 800 nm, upon excitation at 420 nm.

Bacterial culture

Bacterial cells were inoculated from −80°C frozen tubes onto LB agar plates and incubated overnight at 37°C for *E. coli*, MDR *E. coli*, and *S. aureus*. Cells from single colonies were transferred to liquid LB medium and incubated at 37°C in a MaxQ 4000 & Heidolph Incubator Shaker at 220 rpm/min overnight.

Membrane potential and permeability assay

Both *E. coli* and *S. aureus* with a concentration of 10^8 CFU/ml were incubated with the desired concentration of antibiotics, TPA2PyBu, and CCCP for 30 min. Cells were then stained with the BacLight Bacterial Membrane Potential kit. This kit uses $DiOC_2(3)$ to measure cell membrane potential as a ratio of green (λ_{ex} = 488 nm, λ_{em} = 525/50 nm) to red (λ_{ex} = 488 nm, λ_{em} = 610/20 nm). Membrane integrity was measured by staining cells with TO-PRO-3, a dye that is excluded from cells with an intact membrane (λ_{ex} = 640 nm ex, λ_{em} = 670/30 nm). The fluorescent intensities of $DiOC_2(3)$ and TO-PRO-3 were measured by the CytoFLEX flow cytometry platform (Beckman Coulter) to assess the effects of TPA2PyBu, CCCP, and antibiotics on bacteria. Each data file recorded 10,000 events, and subsequent analysis was conducted using FlowJo v10 software.

Mammalian cell cytotoxicity

For the cytotoxicity study, Raw 264.7, HEK-293, Hela, and NIH/3T3 cells were seeded in 96-well plates overnight at 37°C. After 24 hours, cells were treated with TPA2PyBu at various concentrations and incubated for 48 hours. After that, the culture medium was replaced by a fresh one containing CCK-8 and incubated for 2 hours. Absorption was read in a BioTech Synergy H4 at a wavelength of 450 nm.

Confocal imaging of lab bacterial strains

Ten microliters of overnight cultured *E. coli* and *S. aureus* was transferred to 5-ml fresh LB medium and incubated at 37°C under shaking (220 rpm/min). Upon reaching the logarithmic phase with OD_{600} (optical density at 600 nm) ~ 0.5, both *E. coli* and *S. aureus* were harvested by centrifugation at 3000 rpm for 3 min and resuspended in PBS to OD_{600} ~ 0.1. Subsequently, the bacteria solutions were treated with TPA2PyBu (2 μM) for 30 min. Twenty microliters of TPA2PyBu-treated bacteria cells was dropped onto the center of the cover glass and allowed to adhere at room temperature for 30 min, to allow cell adherence. Cover glasses were then covered onto glass slides for CLSM imaging.

MIC assay

Mid-exponential phase (OD_{600} = 0.4 to 0.6) *S. aureus* or *E. coli* cultures were diluted in LB medium containing various concentrations (0, 0.2, 0.5, 1, 2, 5, 10, 20, and 50 μM) of TPA2PyCHO, TPA2PyMe, TPA2PyEt, TPA2PyBu, and TPA2PyHex at a final concentration of ~10^5 CFU/ml. The obtained dilutions were inoculated in 96-well plates and incubated at 37°C for 14 hours. MIC was recorded at the lowest concentration of the compound which results in no visible bacterial growth.

Serial passaging assay to evolve resistance

The drug resistance of *S. aureus* MRSA USA300 was induced by repeated treatment of bacteria with nisin, ciprofloxacin, and TPA2PyBu at sub-MIC. The MICs of nisin, ciprofloxacin, and TPA2PyBu against *S. aureus* MRSA USA300 were determined after 14 hours of incubation at 37°C. Cells cultured in 0.5 × MIC of the specified antibiotics and TPA2PyBu were then transferred to an antibiotic-free medium, followed by a reassessment of the MIC. This single-passage procedure was iterated 20 times, with cells from each passage preserved as frozen stock. Resistance was confirmed by assessing the MICs of resistant mutants compared to those of *S. aureus* MRSA USA300 that had not been previously exposed to the indicated antibiotics and TPA2PyBu.

Bacterial cytological profiling

Following the protocol described by Nonejuie *et al.* (*47*), overnight cultured *E. coli* and *S. aureus* were diluted 1:100 with fresh LB culture

medium and incubated at 37°C for 1.5 hours on a shaker. Subsequently, cultures were treated with TPA2PyBu at MIC for 30 min at 37°C with slight shaking. After treatment with TPA2PyBu, both *E. coli* and *S. aureus* were stained with Hoechst (1 μg/ml), SYTOX Green (1 μM), and FM4-64 (5 μg/ml) for 10 min at 37°C with slight shaking. Last, bacterial cells were collected by centrifuging at 3000 rpm for 3 min and resuspended in PBS. Bacterial cells were spotted on a cover glass for imaging. Images were collected on a Leica TCS SP8 microscope.

RNA sequencing

S. aureus (~ 10^5 CFU/ml) was incubated in LB culture medium containing 0.25 μM TPA2PyBu ($^1/_4$ MIC) at 37°C for 24 hours before being harvested for total RNA extraction using TRIzol reagent (Invitrogen, CA, USA). The *S. aureus* in the control group was treated under the same condition without TPA2PyBu. Subsequent RNA sequencing was conducted using the HiSeq 4000 SBS Kit (300 cycles; Illumina, CA, USA). Data analysis used FastqStat.jar (v0.11.4) and RSeQC (v2.6.4). Gene functions were assessed through GO (http://www.geneontology.org) and the KEGG (http://www.genome.jp/kegg/). Differential gene expression analysis was carried out using the R package edgeR (v3.24). Genes displaying $|\log_2$ fold change $| > 1$ (with a P value of <0.05) were identified as differentially expressed.

In vivo imaging of bacteria

Experiment protocols involving animals were authorized by the Xiamen University Laboratory Animal Research Center (approval number: XMULAC20230259). The Xiamen University Laboratory Animal Research Center provided balb/c mice (6 to 7 weeks of age). The mice were anesthetized with isofluorane, and the hair on the thigh and back was removed. A suspension of *S. aureus* (10^8 CFUs) was injected under the right rear thigh skin (injection in 50 μl of LB), 30 μl of turpentine was injected under the left rear thigh skin, and Hela cells (10^6 cells) were injected in the shoulder regions. Animals were anesthetized with isofluorane, given a tail vein injection of TPA2PyBu and imaged at 1-, 2-, 4-, and 6-hour time points. Fluorescence images were captured using an IVIS Lumina Imaging System. The fluorescence intensity from the area around the bacterial or saline injection site (region of interest) was integrated.

Statistical analysis

Differences between the treatment and control arms were analyzed using either one-way or two-way analysis of variance (ANOVA) and post hoc Tukey's test. P values of < 0.05 were considered statistically significant.

Supplementary Materials

The PDF file includes:
Supplementary Materials and Methods
Figs. S1 to S26
References

Other Supplementary Material for this manuscript includes the following:
Data S1

REFERENCES AND NOTES

1. U. Hofer, The cost of antimicrobial resistance. *Nat. Rev. Microbiol.* **17**, 3 (2019).
2. C. Nathan, O. Cars, Antibiotic resistance—Problems, progress, and prospects. *N. Engl. J. Med.* **371**, 1761–1763 (2014).
3. B. Aslam, W. Wang, M. I. Arshad, M. Khurshid, S. Muzammil, M. H. Rasool, M. A. Nisar, R. F. Alvi, M. A. Aslam, M. U. Qamar, M. K. F. Salamat, Z. Baloch, Antibiotic resistance: A rundown of a global crisis. *Infect. Drug Resist.* **11**, 1645–1658 (2018).
4. E. D. Brown, G. D. Wright, Antibacterial drug discovery in the resistance era. *Nature* **529**, 336–343 (2016).
5. T. M. Privalsky, A. M. Soohoo, J. Wang, C. T. Walsh, G. D. Wright, E. M. Gordon, N. S. Gray, C. Khosla, Prospects for antibacterial discovery and development. *J. Am. Chem. Soc.* **143**, 21127–21142 (2021).
6. J. O'Neill, *Antimicrobial Resistance: Tackling a Crisis for the Health and Wealth of Nations* (Review on Antimicrobial Resistance, 2014).
7. K. McKeage, Finafloxacin: First global approval. *Drugs* **75**, 687–693 (2015).
8. L. B. Randall, E. Georgi, G. H. Genzel, H. P. Schweizer, Finafloxacin overcomes Burkholderia pseudomallei efflux-mediated fluoroquinolone resistance. *J. Antimicrob. Chemother.* **72**, 1258–1260 (2017).
9. L. L. Ling, T. Schneider, A. J. Peoples, A. L. Spoering, I. Engels, B. P. Conlon, A. Mueller, T. F. Schäberle, D. E. Hughes, S. Epstein, M. Jones, L. Lazarides, V. A. Steadman, D. R. Cohen, C. R. Felix, K. A. Fetterman, W. P. Millett, A. G. Nitti, A. M. Zullo, C. Chen, K. Lewis, A new antibiotic kills pathogens without detectable resistance. *Nature* **517**, 455–459 (2015).
10. L. L. Silver, Multi-targeting by monotherapeutic antibacterials. *Nat. Rev. Drug Discov.* **6**, 41–55 (2007).
11. J. G. Hurdle, A. J. O'Neill, I. Chopra, R. E. Lee, Targeting bacterial membrane function: An underexploited mechanism for treating persistent infections. *Nat. Rev. Microbiol.* **9**, 62–75 (2011).
12. J. M. A. Blair, M. A. Webber, A. J. Baylay, D. O. Ogbolu, L. J. V. Piddock, Molecular mechanisms of antibiotic resistance. *Nat. Rev. Microbiol.* **13**, 42 (2014).
13. F. R. Greten, S. I. Grivennikov, Inflammation and cancer: Triggers, mechanisms, and consequences. *Immunity* **51**, 27–41 (2019).
14. X. Ning, S. Lee, Z. Wang, D. Kim, B. Stubblefield, E. Gilbert, N. Murthy, Maltodextrin-based imaging probes detect bacteria in vivo with high sensitivity and specificity. *Nat. Mater.* **10**, 602–607 (2011).
15. T. Zhao, J. Zhang, X. Han, J. Yang, X. Wang, M. Vercruysse, H.-Y. Hu, X. Lei, A pseudopaline fluorescent probe for the selective detection of Pseudomonas aeruginosa. *CCS Chemistry* **3**, 2405–2417 (2021).
16. M. A. Sellmyer, I. Lee, C. Hou, C.-C. Weng, S. Li, B. P. Lieberman, C. Zeng, D. A. Mankoff, R. H. Mach, Bacterial infection imaging with [^{18}F]fluoropropyl-trimethoprim. *Proc. Natl. Acad. Sci. U.S.A.* **114**, 8372–8377 (2017).
17. E. A. Weinstein, A. A. Ordonez, V. P. DeMarco, A. M. Murawski, S. Pokkali, E. M. MacDonald, M. Klunk, R. C. Mease, M. G. Pomper, S. K. Jain, Imaging Enterobacteriaceae infection in vivo with ^{18}F-fluorodeoxysorbitol positron emission tomography. *Sci. Transl. Med.* **6**, 259ra146 (2014).
18. M. M. Welling, A. W. Hensbergen, A. Bunschoten, A. H. Velders, H. Scheper, W. K. Smits, M. Roestenberg, F. W. B. van Leeuwen, Fluorescent imaging of bacterial infections and recent advances made with multimodal radiopharmaceuticals. *Clin. Transl. Imaging* **7**, 125–138 (2019).
19. M. van Oosten, T. Schäfer, J. A. C. Gazendam, K. Ohlsen, E. Tsompanidou, M. C. de Goffau, H. J. M. Harmsen, L. M. A. Crane, E. Lim, K. P. Francis, L. Cheung, M. Olive, V. Ntziachristos, J. M. van Dijl, G. M. van Dam, Real-time in vivo imaging of invasive- and biomaterial-associated bacterial infections using fluorescently labelled vancomycin. *Nat. Commun.* **4**, 2584 (2013).
20. J. Liang, B. Z. Tang, B. Liu, Specific light-up bioprobes based on AIEgen conjugates. *Chem. Soc. Rev.* **44**, 2798–2811 (2015).
21. G. Qi, X. Liu, L. Shi, M. Wu, J. Liu, B. Liu, Enzyme-mediated intracellular polymerization of AIEgens for light-up tumor localization and theranostics. *Adv. Mater.* **34**, e2106885 (2022).
22. X. Cai, B. Liu, Aggregation-induced emission: Recent advances in materials and biomedical applications. *Angew. Chem. Int. Ed. Engl.* **59**, 9868–9886 (2020).
23. M. Kang, C. Zhou, S. Wu, B. Yu, Z. Zhang, N. Song, M. M. S. Lee, W. Xu, F.-J. Xu, D. Wang, L. Wang, B. Z. Tang, Evaluation of structure–function relationships of aggregation-induced emission luminogens for simultaneous dual applications of specific discrimination and efficient photodynamic killing of Gram-positive bacteria. *J. Am. Chem. Soc.* **141**, 16781–16789 (2019).
24. G. Qi, F. Hu, L. S. Kenry, M. Wu, B. Liu, An AIEgen-peptide conjugate as a phototheranostic agent for phagosome-entrapped bacteria. *Angew. Chem. Int. Ed Engl.* **58**, 16229–16235 (2019).
25. G. Qi, F. Hu, K. C. C. Kenry, M. Wu, Y. H. Gan, B. Liu, Bacterium-templated polymer for self-selective ablation of multidrug-resistant bacteria. *Adv. Funct. Mater.* **30**, 2001338 (2020).
26. F. Hu, G. Qi, Kenry, D. Mao, S. Zhou, M. Wu, W. Wu, B. Liu, Visualization and in situ ablation of intracellular bacterial pathogens through metabolic labeling. *Angew. Chem. Int. Ed. Engl.* **59**, 9288–9292 (2019).
27. J. Xie, Y. Wang, W. Choi, P. Jangili, Y. Ge, Y. Xu, J. Kang, L. Liu, B. Zhang, Z. Xie, J. He, N. Xie, G. Nie, H. Zhang, J. S. Kim, Overcoming barriers in photodynamic therapy harnessing nano-formulation strategies. *Chem. Soc. Rev.* **50**, 9152–9201 (2021).
28. D. Novo, N. G. Perlmutter, R. H. Hunt, H. M. Shapiro, Accurate flow cytometric membrane potential measurement in bacteria using diethyloxacarbocyanine and a ratiometric technique. *Cytometry* **35**, 55–63 (1999).

29. R. R. Chaudhuri, A. G. Allen, P. J. Owen, G. Shalom, K. Stone, M. Harrison, T. A. Burgis, M. Lockyer, J. Garcia-Lara, S. J. Foster, S. J. Pleasance, S. E. Peters, D. J. Maskell, I. G. Charles, Comprehensive identification of essential Staphylococcus aureus genes using Transposon-Mediated Differential Hybridisation (TMDH). *BMC Genomics* **10**, 291 (2009).
30. G. M. Clore, V. Venditti, Structure, dynamics and biophysics of the cytoplasmic protein-protein complexes of the bacterial phosphoenolpyruvate: Sugar phosphotransferase system. *Trends Biochem. Sci.* **38**, 515–530 (2013).
31. J. Deutscher, C. Francke, P. W. Postma, How phosphotransferase system-related protein phosphorylation regulates carbohydrate metabolism in bacteria. *Microbiol. Mol. Biol. Rev.* **70**, 939–1031 (2006).
32. W. Kundig, S. Ghosh, S. Roseman, Phosphate bound to histidine in a protein as an intermediate in a novel phospho-transferase system. *Proc. Natl. Acad. Sci. U.S.A.* **52**, 1067–1074 (1964).
33. H. Lebrette, E. Borezée-Durant, L. Martin, P. Richaud, E. Boeri Erba, C. Cavazza, Novel insights into nickel import in Staphylococcus aureus: The positive role of free histidine and structural characterization of a new thiazolidine-type nickel chelator. *Metallomics* **7**, 613–621 (2015).
34. B. A. Smith, W. J. Akers, W. M. Leevy, A. J. Lampkins, S. Xiao, W. Wolter, M. A. Suckow, S. Achilefu, B. D. Smith, Optical imaging of mammary and prostate tumors in living animals using a synthetic near infrared zinc(II)-dipicolylamine probe for anionic cell surfaces. *J. Am. Chem. Soc.* **132**, 67–69 (2010).
35. W. M. Leevy, S. T. Gammon, H. Jiang, J. R. Johnson, D. J. Maxwell, E. N. Jackson, M. Marquez, D. Piwnica-Worms, B. D. Smith, Optical imaging of bacterial infection in living mice using a fluorescent near-infrared molecular probe. *J. Am. Chem. Soc.* **128**, 16476–16477 (2006).
36. T. Mahfouz, M. H. Miceli, F. Saghafifar, S. Stroud, L. Jones-Jackson, R. Walker, M. L. Grazziutti, G. Purnell, A. Fassas, G. Tricot, B. Barlogie, E. Anaissie, 18F-fluorodeoxyglucose positron emission tomography contributes to the diagnosis and management of infections in patients with multiple myeloma: A study of 165 infectious episodes. *J. Clin. Oncol.* **23**, 7857–7863 (2005).
37. S. Liu, B. Wang, Y. Yu, Y. Liu, Z. Zhuang, Z. Zhao, G. Feng, A. Qin, B. Z. Tang, Cationization-enhanced type I and type II ROS generation for photodynamic treatment of drug-resistant bacteria. *ACS Nano* **16**, 9130–9141 (2022).
38. G. Qi, Y. Tang, L. Shi, J. Zhuang, X. Liu, B. Liu, Capsule shedding and membrane binding enhanced photodynamic killing of Gram-negative bacteria by a unimolecular conjugated polyelectrolyte. *Nano Lett.* **23**, 10374–10382 (2023).
39. Y. W. Yu, Y. B. Liu, Y. T. Chen, J. K. Chen, G. X. Feng, B. Z. Tang, Cationic AIE-active photosensitizers for highly efficient photodynamic eradication of drug-resistant bacteria. *Mater. Chem. Front.* **7**, 96–105 (2022).
40. G. Qi, X. Liu, L. Shi, J. Zhuang, B. Liu, Targeted depletion of individual pathogen by bacteria-templated polymer. *Adv. Mater.* **36**, e2307940 (2024).
41. Z. Li, J. Song, X. Gao, X. Ma, K. Liu, Z. Ma, Q. Wang, X. Zeng, H. Zhang, P. Zhang, H. Guo, J. Yin, Highly efficient green light-excited AIE photosensitizers derived from BF2-curcuminoid for specific photodynamic eradication of Gram-negative bacteria. *Chin. Chem. Lett.* **36**, 110073 (2025).
42. H. Nature CommunicationsBai, W. He, J. H. C. Chau, Z. Zheng, R. T. K. Kwok, J. W. Y. Lam, B. Z. Tang, AIEgens for microbial detection and antimicrobial therapy. *Biomaterials* **268**, 120598 (2021).
43. R. E. W. Hancock, F. S. L. Brinkman, Function of *Pseudomonas* porins in uptake and efflux. *Annu. Rev. Microbiol.* **56**, 17–38 (2002).
44. H. Nikaido, Molecular basis of bacterial outer membrane permeability revisited. *Microbiol. Mol. Biol. Rev.* **67**, 593–656 (2003).
45. M. J. Mitcheltree, A. Pisipati, E. A. Syroegin, K. J. Silvestre, D. Klepacki, J. D. Mason, D. W. Terwilliger, G. Testolin, A. R. Pote, K. J. Y. Wu, R. P. Ladley, K. Chatman, A. S. Mankin, Y. S. Polikanov, A. G. Myers, A synthetic antibiotic class overcoming bacterial multidrug resistance. *Nature* **599**, 507–512 (2021).
46. S. P. Denyer, J. Y. Maillard, Cellular impermeability and uptake of biocides and antibiotics in Gram-negative bacteria. *J. Appl. Microbiol.* **92**, 35S–45S (2002).
47. P. Nonejuie, M. Burkart, K. Pogliano, J. Pogliano, Bacterial cytological profiling rapidly identifies the cellular pathways targeted by antibacterial molecules. *Proc. Natl. Acad. Sci. U.S.A.* **110**, 16169–16174 (2013).
48. H. Wang, W. Ding, G. Wang, C. Pan, M. Duan, G. Yu, Tunable molecular weights of poly(triphenylamine-2,2′-bithiophene) and their effects on photovoltaic performance as sensitizers for dye-sensitized solar cells. *J. Appl. Polym. Sci.* **133**, 44182 (2016).

Acknowledgments

Funding: This study is supported by the National University of Singapore (A-0001423-06-00 to B.L.), the Singapore National Research Foundation (A-0009163-01-00 and E-467-00-0012-02 to B.L.), and the National Natural Science Foundation of China (22105229 to L.S.). **Author contributions:** Conceptualization: G.Q., X.L., and B.L. Methodology: G.Q., X.L., H.L., Y.Q., C.L., and J.Z. Investigation: G.Q., X.L., H.L., Y.Q., C.L., and J.Z. Visualization: G.Q., X.L., H.L., Y.Q., C.L., and J.Z. Funding acquisition: L.S. and B.L. Project administration: L.S. and B.L. Supervision: L.S. and B.L. Writing—original draft: G.Q., X.L., and B.L., Writing—review and editing: All authors. **Competing interests:** The authors declare that they have no competing interests. **Data and materials availability:** All data needed to evaluate the conclusions in the paper are present in the paper and/or the Supplementary Materials. The transcriptomic dataset has been deposited to the NCBI Gene Expression Omnibus (GEO) data repository with the accession ID GSE285871.

Submitted 22 April 2024
Accepted 7 March 2025
Published 11 April 2025
10.1126/sciadv.adp9448